Attosecond electron bunches accelerated and compressed by radially polarized laser pulses and soft-x-ray pulses from optical undulators

2014 J. Phys. B: At. Mol. Opt. Phys. 47 015601

(http://iopscience.iop.org/0953-4075/47/1/015601)

IOP Publishing Journal of Physics B: Atomic, Molecular and Optical Physics
J. Phys. B: At. Mol. Opt. Phys. **47** (2014) 015601 (7pp) doi:10.1088/0953-4075/47/1/015601

Attosecond electron bunches accelerated and compressed by radially polarized laser pulses and soft-x-ray pulses from optical undulators

A Sell[1] **and F X Kärtner**[1,2,3]

[1] Department of Electrical Engineering and Computer Science and Research Laboratory of Electronics, Massachusetts Institute of Technology, 77 Massachusetts Ave., Cambridge, MA-02139, USA
[2] Center for Free-Electron Laser Science, Deutsches Elektronen Synchrotron, and Department of Physics, University of Hamburg, Notkestraße 85, D-22607 Hamburg, Germany
[3] The Hamburg Center for Ultrafast Imaging, Luruper Chaussee 149, D-22761 Hamburg, Germany

E-mail: asell@mit.edu

Received 1 October 2013, revised 1 November 2013
Accepted for publication 8 November 2013
Published 10 December 2013

Abstract

We present a study of direct laser driven electron acceleration and scaling of attosecond bunch compression in unbound vacuum. Simple analytical expressions and detailed three-dimensional numerical calculations including space charge and non-paraxial laser fields reveal the conditions for compression to attosecond electron sheets. Intermediate emittance minima suitable for brilliant x-ray generation in optical undulators are predicted. We verify a favourable coherent enhancement of the resulting x-ray fields and demonstrate feasibility for realistic laser parameters.

(Some figures may appear in colour only in the online journal)

1. Introduction

Ultrashort relativistic electron bunches and brilliant x-ray bursts are expected to open new avenues in ultrafast physics, serving as probes with atomic spatial and attosecond temporal resolution [1]. Applications like ultrafast molecular chemistry, monitoring structural dynamics of physical and dynamical processes and phase-contrast imaging fuel the ever growing demand for beamtime at synchrotrons and free-electron lasers and drive a quest for laboratory scale sources [2].

Electron bunches in the order of 10 fs have been achieved with plasma-wakefield accelerators [3, 4]. Recently, incoherent high-energy emission from optical undulators (OPU) has been demonstrated using a 100 TW driving laser [5]. Certain properties of the wakefield technique, like instabilities of the nonlinear interactions or a plasma-limited compression rate, currently limit the bunch quality and therefore prevent coherent enhancement in OPUs. On the other hand, few-femtosecond bunches have been predicted for vacuum laser acceleration approaches exploiting the ponderomotive force [6, 7]. However, the efficiency of this indirect laser–electron-interaction is limited, and quiver motions distort the transverse phase space [8].

Recent work on direct laser acceleration shows promise in overcoming these issues: The axial electric field of radially polarized pulses efficiently accelerates electrons, whereas the radial fields provide transverse confinement [9]. Extensive work on single electrons travelling on-axis has shown the feasibility of the acceleration concept [10–12], and has unveiled the potential of accelerated electron bunches for coherent Thomson-scattering employing complicated laser driving pulse shapes [13]. Three-dimensional simulations have predicted electron bunch compression, however without considering space charge and emittance effects or by employing paraxial approximations of the driving field [14–16]. A recent study has demonstrated the invalidity of the paraxial approximation for a broad range of laser and bunch parameters [17].

Here, we propose a general scheme to generate low-emittance attosecond electron bunches to produce brilliant

coherent x-ray bursts in a laser undulator. Our example yielding 2 as bunches at 5.2 MeV assumes Gaussian laser pulses with a moderate pulse energy of 50 mJ which might soon be available even at multi-kHz repetition rates. We give a physical understanding and scaling of the bunch compression, and investigate the influence of space charge, transverse dynamics and particle statistics. We find intermediate acceleration phases exposing extremely low-emittance values at high electron energies. Our numerical simulations use a relativistic three-dimensional model, including space charge effects and the electromagnetic emission from the accelerated particles. Assuming a combination of a non-paraxial radially polarized pulse for the compression and acceleration and a counter-propagating linear polarized Gaussian pulse for the inverse Compton scattering process in the OPU, we discuss the coherent properties of the resulting attosecond x-ray pulses.

In comparison to high-harmonic generation (HHG) as an alternative means of generating soft x-ray bursts [18, 19], coherent OPUs promise an energy scaling without significant changes in efficiency (see last section). The predicted number of 1.9×10^5 photons at an energy of 0.53 keV is similar to current HHG results. However, HHG pulses are strongly chirped so their potentially short pulse duration cannot be exploited. The spectral phase of x-ray pulses from OPUs is nearly constant, so their duration (75 as) is set solely by the output photon energy and the number of cycles of the OPU laser.

2. Laser acceleration and bunch compression

Bunch compression very naturally arises in direct laser acceleration in unbound vacuum due to the so-called 'snowplough effect': assuming a fixed time for each electron to get accelerated from an initial velocity $\beta_\mathrm{i}(=v_\mathrm{i}/c)$ to the final velocity β_f, a field travelling with the speed of light c takes the time $T_\mathrm{cpt} = L_\mathrm{i}c^{-1}/(1-\beta_\mathrm{i})$ to traverse a bunch of length L_i. The final bunch extension is given by the velocity mismatch between field and electrons [20]

$$L_\mathrm{f} = (\beta_\phi - \beta_\mathrm{f})cT_\mathrm{cpt} = \frac{\beta_\phi - \beta_\mathrm{f}}{1-\beta_\mathrm{i}}L_\mathrm{i} \approx \frac{1}{2\gamma_\mathrm{f}^2}\frac{1}{1-\beta_\mathrm{i}}L_\mathrm{i}, \qquad (1)$$

with the approximation $\gamma_\mathrm{f} \gg 1$ (with $\gamma = 1/\sqrt{1-\beta^2}$) and $\beta_\phi \equiv 1$, for now. For $\beta_\mathrm{f} > \beta_\mathrm{i}$ the bunch obviously compresses, even in its rest frame where there is no relativistic contraction. From (1) we obtain a temporal compression factor η of

$$\eta = \frac{\beta_\mathrm{i}L_\mathrm{f}}{\beta_\mathrm{f}L_\mathrm{i}} = \frac{1-\beta_\phi\beta_\mathrm{f}^{-1}}{1-\beta_\mathrm{i}^{-1}} \approx \frac{1}{2\gamma_\mathrm{f}^2}\frac{1}{\beta_\mathrm{i}^{-1}-1}. \qquad (2)$$

Note that the wavelength achieved by OPUs from an initial wavelength of λ_OPU scales approximately as

$$\lambda_\text{x-ray} \approx \frac{\lambda_\mathrm{OPU}}{4\gamma_\mathrm{f}^2} \qquad (3)$$

and stays matched to the bunch length (also $\propto \gamma_\mathrm{f}^{-2}$) while scaling the energy of the proposed coherent scheme. Compression gets deteriorated mainly by space charge, radial field inhomogeneities, and the initial electron momentum distribution. In the following sections, we identify situations where L_f is minimized.

Our radially polarized acceleration laser is described as a TM_{01}-beam [16] without employing paraxial approximations, using Gaussian parameters (w_0: waist radius, $k_0 = \omega/c$: wave number, t_0: pulse duration, Ψ_0: phase). In cylindrical coordinates (r, ϕ, z) the nonzero field components at time t are computed by

$$\begin{aligned}
\kappa &= k_0\sqrt{r^2 + (z + \mathrm{i}a)^2} \\
a &= \frac{1}{k_0}\sqrt{\left(\frac{1}{2}(k_0w_0)^2 + 1\right)^2 - 1} \\
\mathcal{E} &= E_0 \exp\left[\mathrm{i}(k_0ct + \Psi_0) - k_0a\right] \cdot \operatorname{sech}\left(\frac{ct-z}{ct_0}\right) \\
E_r^\mathrm{ex} &= \Re\{\mathcal{E}k_0^2 r(a - \mathrm{i}z)j_2(\kappa)\kappa^{-2}\}
\end{aligned} \qquad (4)$$

$$E_z^\mathrm{ex} = \Re\left\{-\frac{2}{3}\mathrm{i}\mathcal{E}\left[j_0(\kappa) + \left(1 - \frac{3k_0^2r^2}{2\kappa^2}\right)j_2(\kappa)\right]\right\} \qquad (5)$$

$$cB_\phi^\mathrm{ex} = \Re\left\{\mathcal{E}k_0 r j_1(\kappa)\kappa^{-1}\right\}, \qquad (6)$$

where j_i denotes spherical Bessel functions of order i, κ is a complex valued normalized radius, and a is the confocal parameter and might be used to determine the degree of paraxiality. Note that the solution given above—except for its temporal envelope—represents an exact solution to the Helmholtz equation. The factor E_0 is determined from the given energy W of the laser pulse as follows [16]:

$$\begin{aligned}
E_0 = 2k_0^{5/2}a^{3/2}\sqrt{\frac{W}{\pi\varepsilon_0 ct_0}}\Bigg[k_0a - \frac{1}{2} - (2(k_0a)^2 - 1)\,\mathrm{e}^{-2k_0a} \\
- \left(k_0a + \frac{1}{2}\right)\mathrm{e}^{-4k_0a}\Bigg]^{-1/2}.
\end{aligned} \qquad (7)$$

The impact of the paraxial approximation of (4)–(6) on electron acceleration simulations has been studied for some time [15]. Recently it has been shown that the cancellation of transverse forces due to an artificial symmetry between E_r^ex and cB_ϕ^ex causes significant deviations in the predicted bunch properties [17]. Thus, here we incorporate the exact solutions, which call for a more careful optimization of the laser parameters than used in our preliminary computations with paraxial fields [21] to achieve low-emittance electron bunch compression.

On the centre axis ($r = 0$) the radial field E_r^ex vanishes, and E_z^ex leads to direct acceleration. Equation (5) yields a phase velocity β_ϕ above the speed of light:

$$\beta_\phi \approx \left[1 - \frac{4c^2}{\omega^2w^2}\right]^{-1} > 1, \qquad (8)$$

where $w^2 = w_0^2(1 + z^2/z_\mathrm{R}^2)$ is the beam diameter, $z_\mathrm{R} = k_0w_0^2/2$ is the Rayleigh length, and the approximation $k_0a \gg 1$ has been used to simplify the equation. The electrons travel with $\beta_\mathrm{el.} < 1$ and thus slip through acceleration periods of the accelerating field. We estimate the phase slip time T_slip assuming a mainly constant electron energy during one acceleration cycle by

$$T_\mathrm{slip}(\beta_\phi - \beta_\mathrm{el.}) = 2\pi/\omega. \qquad (9)$$

3. Numerical model

The equations of motion for each macro-particle with velocity $\vec{\beta}$ and position $\vec{R}$ are

$$\mathrm{d}_{ct}(\vec{\beta}\gamma) = \frac{q}{m_0 c^2}[(\vec{E}^{\mathrm{ex}} + \vec{E}^{\mathrm{in}}) + \vec{\beta} \times c(\vec{B}^{\mathrm{ex}} + \vec{B}^{\mathrm{in}})]$$
$$\mathrm{d}_{ct}\vec{R} = \vec{\beta} = \vec{\beta}\gamma/\sqrt{1+(\beta\gamma)^2}, \quad (10)$$

where m_0 and q are the rest mass and charge of the electrons forming the particle. Many studies solve equations for $\mathrm{d}_t\vec{\beta}$ instead of (10), causing numerical problems for $\beta \to 1$. Our simulation code dealing with the **A**cceleration of **L**aser **D**riven **E**lectron **B**unches **A**nd **RA**diatio**N** of **X**-rays (Aldebaran-X) incorporates an adaptive Runge–Kutta solver of fifth-order with an fourth-order embedded error-estimator [22]. The C++ code utilizes multiple computing kernels via 'OpenMP' and massively parallel graphics processors via 'OpenCL'.

The external fields are computed according to (4)–(6) and (12)–(13) (see below). The internal fields $\vec{E}_n^{\mathrm{in}}$ and $\vec{B}_n^{\mathrm{in}}$, acting on macro-particle n, are calculated by summing the Lorentz-transforms of the Coulomb fields evaluated in the rest frames of all particles $m \neq n$. The resulting equations read

$$\vec{E}_n^{\mathrm{in}} = \frac{1}{4\pi\varepsilon_0}\sum_{m\neq n} q_m\gamma_m\vec{R}_{nm}\left(R'^2_{nm}+\delta^2\right)^{-3/2}$$
$$c\vec{B}_n^{\mathrm{in}} = \frac{1}{4\pi\varepsilon_0}\sum_{m\neq n} q_m\gamma_m\vec{\beta}_m \times \vec{R}_{nm}\left(R'^2_{nm}+\delta^2\right)^{-3/2}. \quad (11)$$

Here $\vec{R}_{nm} = \vec{R}_n - \vec{R}_m$ is the lab-frame particle distance, $R'^2_{nm} = R^2_{nm} + (\gamma_m\vec{\beta}_m\vec{R}_{nm})^2$ is the squared distance in the rest frame of particle m, and ε_0 is the vacuum permittivity. δ is a small constant which is set according to the average macro-particle radius and which is introduced to model the particle's finite extension and charge density.

This direct computational approach was chosen despite its $\mathcal{O}(N^2)$ scaling with the particle number N, since it is accurate for arbitrarily complex bunch shapes and relativistic energy spreads of the electrons—a situation which is very challenging i.e. for particle-in-cell algorithms. Our implementation yields a processing speed of more than 100 GFLOP/s on the graphics processor of the notebook used for the calculations throughout the paper. To achieve an even higher performance of the space charge solver, a hierarchical method might be implemented where particles get lumped for evaluating long-range interactions [23].

4. Bunch compression dynamics

We consider an accelerator geometry, where electron bunches with an energy of $W_0 = 100\,\mathrm{keV}$ (i.e. from a dc electron gun) get injected. This non-relativistic energy yields similar results as acceleration from rest, but avoids issues like creating a bunch in the laser focus and excessive space charge effects [8, 15]. We assume a ellipsoidal bunch, both in real and momentum space. All rest-frame diameters are set to $d_{x,y,z} = 2\,\mu\mathrm{m}$ and $d_{px,py,pz}/(m_0c) = 0.02$, respectively, in order to account for a strong focusing. These parameters are very challenging, only recently bunch durations shorter than the 12 fs assumed here have been demonstrated by field emission from nano-tips [24]. Appropriate charges might be obtained from arrays of tips. Since the acceleration limits the transverse diameter to the order of $w/\sqrt{2}$ by repelling electrons outside of this range, even transverse extended initial bunches eventually are suited for our scheme. An injection parameter z_0 defines the time $ct = -z_0/\beta_{\mathrm{i}}$, at which the bunch with the phase space diameters as given above would reach the origin $z = 0$ without any external fields. A moderate 3.5 TW acceleration laser with a wavelength of $\lambda_{\mathrm{ac}} = 2\pi c/\omega = 2.9\,\mu\mathrm{m}$, a FWHM pulse duration of 13 fs ($t_0 = 7.2\,\mathrm{fs}$, corresponding to a 1.35 cycle pulse) and an energy of 50 mJ is assumed in the rest of the paper.

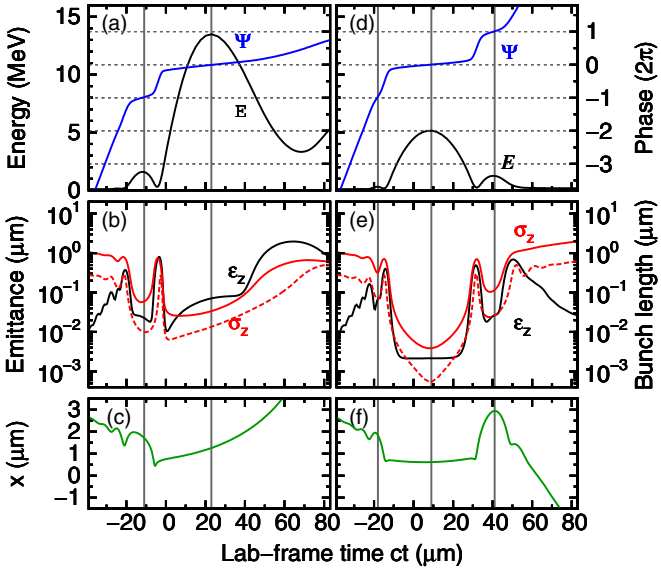

Figure 1. Evolution of (a) and (d) centre bunch energy (black) and on-axis phase Ψ (blue), (b) and (e) bunch emittance ϵ_z (black) and length σ_z (red), and (c) and (f) transverse position x of one particle at the bunch equator. Laser phase Ψ_0, waist radius w_0 and injection offset z_0 are optimized for a final electron energy of 8.8 MeV (a)–(c) or for minimum intermediate bunch length σ_z (d)–(f). Vertical grey lines indicate acceleration phases between slippage events. Initial bunch parameters: $W_0 = 100\,\mathrm{keV}$, $N = 16\,384$; solid lines: $d_{x,y,z} = 2\,\mu\mathrm{m}$, $d_{px,py,pz}/(m_0c) = 0.02$, $Q = -0.2$ pCb; dashed lines: $d_{x,y} = 1\,\mu\mathrm{m}$, $d_z = 0.5\,\mu\mathrm{m}$, $d_{px,py}/(m_0c) = 0.01$, $d_{pz}/(m_0c) = 0.002$, $Q = -10$ fCb.

Figure 1(a) shows the average electron energy and the central laser phase Ψ as evolving with time ct. For this simulation a number of $N = 16\,384$ macro-particles has been used, the results have been confirmed to be stable against a further increase of the particle count. We set the laser parameters to $w_0 = 6.6\,\mu\mathrm{m}$, $z_0 = -5.5\,\mu\mathrm{m}$ and $\Psi_0 = 0.31$ for a maximized final average bunch energy of 8.8 MeV [11, 12]. Vertical grey lines mark maxima in energy, corresponding to 2π-multiples of the phase. The main acceleration takes place while the phase approaches $\Psi = 0$. Assuming a slippage time of $cT_{\mathrm{slip}} = 34\,\mu\mathrm{m}$ and highest phase velocity, (8) and (9) yield an average longitudinal electron energy of only 0.9 MeV, which is a factor of 15 below the peak energy, partially because strong transverse motions contribute to the simulated value as well.

Figure 1(b) depicts the normalized rms emittance ϵ_z and the rms bunch length $\sigma_z = \sqrt{\langle z^2\rangle - \langle z\rangle^2}$. We use the standard definition $\epsilon_u = \frac{1}{m_0 c}\sqrt{\langle u^2\rangle_c \langle p_u^2\rangle_c - \langle u p_u\rangle_c^2}$ where $\langle fg\rangle_c = \langle fg\rangle - \langle f\rangle\langle g\rangle$ is a centred average over all particles and (u, p_u) with $u \in \{x, y, z\}$ denote Cartesian coordinates and momenta. For relativistic energy spreads the rms emittance generally is not a conserved quantity, even without considering space charge and external fields. This is because z changes with β_z, which is a nonlinear function of $p_z = m_0 c\gamma\beta_z$. Thus, the phase volume deforms, and ϵ changes without violating Liouville's theorem.

The 200-fold increase of emittance seen in figure 1(b) appears mainly in the main acceleration phase and the subsequent slippage event, where the transversely expanding bunch (see figure 1(c)) samples an increasing cross-section of the accelerating field. σ_z stays smaller, which we attribute to the high peak electron energies and the compression factor as given in (1). A reduced initial bunch emittance and a reduced charge of the bunch lead only to minor improvements of σ_z, as depicted by the dashed line in figure 1(b). The strong emittance-growth limits the usefulness of laser accelerated bunches for coherent OPUs and other schemes which call for extremely well-controlled bunch parameters.

The aforementioned issues are solved by choosing a different set of laser parameters. An optimization procedure as detailed in the next section leads to a laser phase of $\Psi_0 = 1.375$, an injection timing $z_0 = -5.4\,\mu$m and an increased beam waist radius of $w_0 = 8.9\,\mu$m, which result in a reduced transverse gradient of the acceleration field over the bunch diameter (figures 1(d)–(f)). The main acceleration cycle, where the electrons experience the biggest gain in energy, still corresponds to $\Psi = 0$, as seen from the blue line in figure (d), and the electrons pass the focus while the peak field arrives. A slippage time of $T_{\text{slip}} = 32\,\mu$m (grey vertical lines) corresponds to an average electron energy of 0.8 MeV which is a factor of 6 below the peak energy. In comparison to figure 1(a), the final energy of 184 keV is smaller by a factor of 50, but whenever Ψ is close to a multiple of 2π, the energy peaks and ϵ_z and σ_z go through pronounced minima which can be exploited for coherent x-ray generation. The highest peak at $ct = 8\,\mu$m exhibits an energy of 5.2 MeV and a normalized longitudinal emittance of 2.1 nm, which is only 10% above the initial value. The bunch is compressed by a factor of $\eta = 1/1300$ to a duration as short as 2 as (dashed line in figure 1(e)). Equation (2) yields a compression of $\eta = 1/200$ since it only applies for static field envelopes. Increasing the bunch charge to -0.2 pCb preserves the dynamics of the bunch statistics but deteriorates the minima of ϵ_z and σ_z (solid lines in figure 1(e)).

Figure 2 shows snapshots of the bunch evolution for theses parameters. The upper half depicts the axial field amplitude, the lower half the radial components. In sub-figure (a), the laser pulse starts catching up with the electron bunch. Slight modulations of the electron density set in, and the emittance starts increasing. Figure (b) shows the bunch while the emittance peaks and the electrons slip from one acceleration phase into the next. Sub-figure (c) sketches the sheet-like electron distribution while the energy peaks and σ_z is minimal.

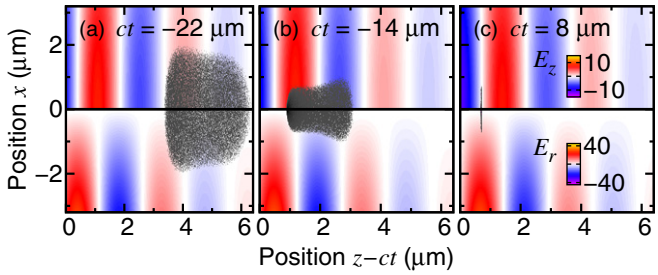

Figure 2. Steps of the acceleration process depicted in the lab-frame. (a) Onset of modulations. (b) Slippage event at an emittance maximum. (c) Acceleration at minimum emittance and bunch duration. Interacting macro-particles are represented by grey dots, normalized transverse (upper panel) and axial (lower panel) electric fields are colour coded (unit: GV m^{-1}). $d_{x,y,z} = 2\,\mu$m, $d_{px,py,pz}/(m_0 c) = 0.02$, $Q = -0.2$ pCb, $N = 65\,536$.

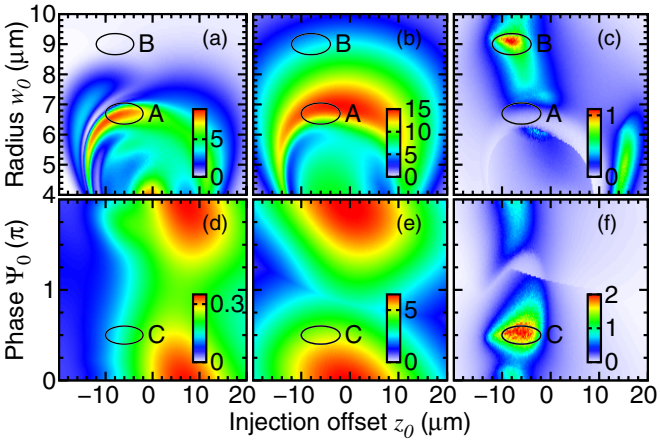

Figure 3. (a)–(c) Variation of laser focal radius w_0 and injection offset z_0 for laser phase $\Psi_0 = 0$. (d)–(f) Variation of z_0 and Ψ_0 for $w_0 = 8.9\,\mu$m. (a) and (d) Final electron energy (MeV). (b) and (e) Peak electron energy during acceleration (MeV). (c) and (f) Peak inverse bunch duration $1/\sigma_z$ during acceleration (1 nm^{-1}). Parameters: $d_{x,y} = 1\,\mu$m, $d_z = 0.5\,\mu$m, $d_{px,py}/(m_0 c) = 0.01$, $d_{pz}/(m_0 c) = 0.002$, $Q = -10$ fCb, $N = 1024$.

We propose using this phase for inverse Compton scattering in the OPU. The computed duration of the bunch already includes curvature and favours the usage of the intermediate energy peaks instead of the final, strongly curved and lower-energy ensemble.

5. Laser parameter optimization

In order to obtain optimum laser and bunch parameters, the focal radius w_0, the laser phase Ψ_0 and the injection offset z_0 are varied. First, $\Psi_0 = 0$ is kept constant, while w_0 and z_0 are allowed to change over a broad range (see figures 3(a)–(c) for selected bunch properties). Each of the 24 000 points in these plots shows a figure of merit (FOM) evaluated in a full simulation run including space charge. To speed up calculations, we use only $N = 1024$ macro-particles. The lower particle count does not affect the results noticeably, as we checked at several test points. In a next step, w_0 is kept constant and z_0 and the phase Ψ_0 are varied (see figures 3(d)–(f) for $w_0 = 8.9\,\mu$m as required for minimum bunch length σ_z).

Iterating the optimization (with the new start value for Ψ_0) does not lead to significant improvements. We choose this optimization order since the influence of Ψ_0 on the resulting bunch dynamics is comparatively smooth, whereas w_0 and z_0 exert stronger influence.

Figures 3(a) and (d) display a colour coded plot of the final electron energies. The maximum is located at negative z_0 and a laser phase Ψ_0 close to zero (the second optimization step with $w_0 = 6.6\,\mu$m is not shown). Only a narrow range of beam diameters (marked as region 'A' in the plots) yields a high final electron energy. In contrast, the peak electron energy (figures 3(b) and (e)) during acceleration reaches values twice as big and covers a much broader parameter range.

We choose a different FOM to optimize the bunch for inverse Compton scattering. According to (3) and the coherence requirement $\lambda_{\text{x-ray}} > \sigma_z$, an obvious choice would be to maximize $1/(\gamma_\text{f}^2\sigma_z)$ of the bunch. However, we find that maximizing just $1/\sigma_z$ gives a very similar result (see figures 3(c) and (f)). To achieve a certain x-ray energy, only points exceeding a minimum value of γ_f are considered in the optimization. As indicated by the circles 'B' and 'C', the region optimal for inverse Compton scattering is clearly disjunct from the region yielding maximum final electron energies. Especially the significantly bigger beam diameter helps avoiding the excessive distortions of the bunch occurring otherwise.

6. X-ray generation in an optical undulator

Finally, we investigate brilliant x-ray generation in OPUs with the optimized bunches. A counter-propagating linearly polarized Gaussian laser field is superimposed to the acceleration laser. Its non-vanishing Cartesian components are given by

$$\begin{aligned}\Psi &= \Psi_0 + \omega(\tau + \zeta/c) + \frac{\zeta}{z_\text{R}}\frac{r^2}{w^2} - \Psi_\text{Gouy}\\ \mathcal{E} &= E_0\frac{w_0}{w}\exp\left(-\frac{r^2}{w^2}\right)\cdot\operatorname{sech}\left(\frac{\tau+\zeta/c}{t_0}\right)\\ E_x^\text{ex} &= -cB_y^\text{ex} = \mathcal{E}\sin(\Psi)\end{aligned} \tag{12}$$

$$yE_z^\text{ex} = -xcB_z^\text{ex} = \mathcal{E}\frac{xyw_0}{wz_\text{R}}\cos\left(\Psi - \Psi_\text{Gouy}\right), \tag{13}$$

where $\zeta = z - z_\text{off}$ and $c\tau = ct - z_\text{off}$ are shifted to allow for selecting the collision timing and position, and $\Psi_\text{Gouy} = \arctan(\zeta/z_\text{R})$ is the Gouy-phase. Since the OPU laser does not significantly contribute to the electron bunch acceleration and compression, we choose a paraxial field representation. For the rest of the paper, we select a wavelength $\lambda_\text{OPU} = 0.8\,\mu$m, a pulse energy of 30 mJ, a beam radius of $w_0 = 5\,\mu$m, a FWHM pulse duration of 32 fs ($t_0 = 18.1$ fs) and a phase $\Psi_0 = 0$.

Besides the electron dynamics, we now also calculate the radiated electric field of each macro-particle by Liennard–Wiechert potentials:

$$\begin{aligned}\vec{E}_\text{rad}(\vec{r},t) &= \frac{q}{4\pi\varepsilon_0}\frac{1}{\xi^3}[\vec{\rho}(1-\vec{\beta}^2+\vec{D}\vec{\alpha}) - \vec{\alpha}(\vec{D}\vec{\rho})]\\ c\vec{B}_\text{rad}(\vec{r},t) &= |\vec{D}|^{-1}(\vec{D}\times\vec{E}_\text{rad}(\vec{r},t))\end{aligned} \tag{14}$$

where $\vec{R}$, $\vec{\beta} = d_{ct}\vec{R}$ and $\vec{\alpha} = d_{ct}\vec{\beta}$ are position, velocity and acceleration of a particle at the retarded time $t_\text{ret} = t - \frac{1}{c}|\vec{D}|$. The other symbols are defined as $\vec{D} = \vec{r} - \vec{R}(t_\text{ret})$, $\xi = |\vec{D}| - \vec{D}\vec{\beta}$, and $\vec{\rho} = \vec{D} - |\vec{D}|\vec{\beta}$. Since $\vec{D}$ is the distance of the particle position at the retarded time to the observation point, above set of equations is implicit in t_ret. Our algorithm tracks the particles at the retarded time t_ret and linearly interpolates the fields to a given set of evaluation points $(\vec{r}, t)$ to avoid solving the implicit equations.

Each interpolation to a given space-time point obviously requires at least two evaluations of (14) for appropriate retarded times t_ret. The simplest approach, storing the results for each particle and each evaluation point $\vec{r}$ in memory for at least one retarded time step, is ruled out by excessive memory requirements. With a typical particle count $N = 10^4$, $M = 10^4$ evaluation points and six field components occupying 8 byte each, 4.8×10^9 bytes would be required. To mitigate this problem, we keep the most recent macro-particle coordinates in a ring-buffer, and interpolate the radiated fields for several times t at once. This method has a slight computational overhead (at the buffer boundaries (14) is evaluated twice), but for a buffer holding 16 steps (with a moderate size of $16 \cdot N \cdot 9 \cdot 8 = 1.2 \times 10^7$ bytes) there is only a 6% increase in the number of function evaluations.

Now, the electron bunch is accelerated by the radially polarized laser as described in the previous chapters, whereas the superimposed counter-propagating linearly polarized beam adds a wiggling motion which leads to x-ray emission. First, we set the offset $z_\text{off} = 8\,\mu$m such that the undulator pulse collides with the electron bunch at the space-time point where it is compressed best.

Figure 4(a) shows the far-field x-ray spectra as a function of the emission angle for a macro-particle count of $N = 8192$ and a total charge of $Q = -10$ fCb. A broadband incoherent background (light blue) is emitted into an angle of about 100 mrad with a chirp from 0.6 to 0.2 keV due to the lower acceleration of off-axis electrons. A spectrally and spatially narrow peak emanates from the coherent superposition of the radiation fields of all particles. The (FWHM) opening angle of 8.7 mrad, as seen in the integrated intensity plotted over the emission angle in figure (c), resembles the Fourier-transform of the transverse bunch shape. A spectral width of 71 eV at a centre energy of 0.53 keV render these photons interesting for applications. Figure 4(b) depicts the on-axis amplitude spectrum (black). The well-behaved spectral phase (blue) corresponds to a pulse duration of 75 as. Depending on the available acceleration laser, the concept is easily adapted to different x-ray ranges due to the favourable scaling of both, compression and output photon energy with γ_f^2 (see (1) and (3)).

The degree of coherence is estimated from the scaling of the integrated squared fields with the number N of macro-particles. Keeping the total charge Q fixed, incoherent radiation yields a scaling as N^{-1} whereas perfectly coherent emission is independent of N as realized in our simulation (see figure 4(d)), where the field is sampled on-axis and therefore even increases as the spatial beam quality improves with the growing particle number. At realistic numbers of $N = 10^5$, the incoherent

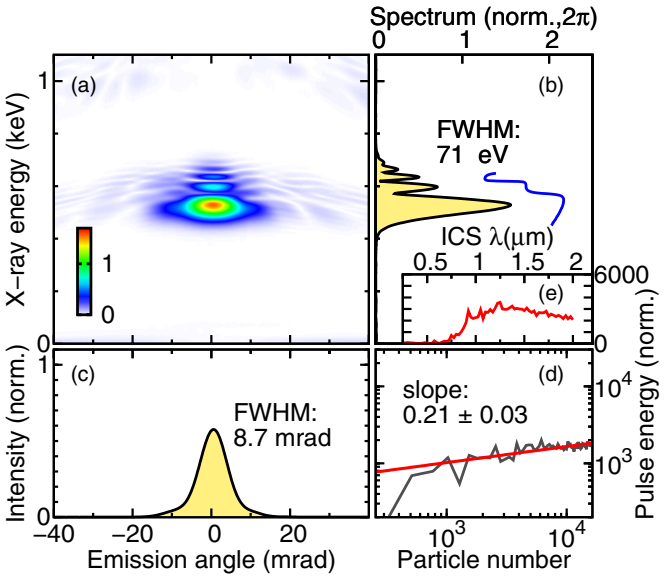

Figure 4. X-ray emission from the accelerated and compressed electron bunch in an optical undulator. (a) X-ray amplitude spectra as a function of emission angle (normalized, colour coded). Parameters: $Q = -10$ fCb, $N = 8192$. (b) X-ray amplitude spectrum on-axis (black, normalized) and phase (blue). (c) Integrated intensity versus emission angle. (d) Coherent scaling (see text). (e) Pulse energy scaling with undulator laser wavelength (see text).

background becomes negligible. Increasing the electron count (i.e. $Q \propto N$), the x-ray power grows as N^2. Even with a low total charge of 10 fCb, as chosen above, we calculate a x-ray pulse energy of 16 pJ (electron to x-ray efficiency: 3×10^{-4}). When increasing the undulator laser wavelength λ_{OPU}, the pulse energy first grows due to relaxing requirements on the bunch, before it reduces due to the increasing x-ray wavelength (see figure 4(e)).

7. Conclusions

In conclusion, we have shown a scheme to achieve 2 as-short relativistic electron bunches by direct laser acceleration using low power lasers. The radially polarized laser beam accelerates the electrons with its axial components, whereas the radial components lead to transverse distortions and confinement of the bunch. By carefully tailoring the laser parameters not for final electron energy (as commonly done) but for intermediate emittance and bunch duration minima, an extremely flat shape of the electron distribution is achieved.

Photons from a near-infrared counter-propagating linearly polarized laser are scattered off the electrons into the x-ray energy range. Due to the favourable properties of the electron distribution, this inverse Compton scattering process is coherently enhanced, allowing for a high conversion efficiency. For realistic laser parameters, we predict 75 as (FWHM) x-ray bursts at a photon energy of 0.53 keV. Our scheme might be employed as a low-emittance attosecond electron and x-ray source for ultrafast studies and for seeding of free-electron lasers.

Acknowledgments

This work has been supported by DARPA AXIS Program under grant N66001-11-1-4192 and by the excellence cluster 'The Hamburg Centre for Ultrafast Imaging—Structure, Dynamics and Control of Matter at the Atomic Scale' of the Deutsche Forschungsgemeinschaft. We thank WS Graves and LJ Wong for helpful discussions and AS acknowledges funding by a Feodor-Lynen fellowship of the Alexander von Humboldt Foundation.

References

[1] Chapman H N 2009 X-ray imaging beyond the limits *Nature Mater.* **8** 299
[2] Graves W S, Brown W, Kärtner F X and Moncton D E 2009 MIT inverse Compton source concept *Nucl. Instrum. Methods Phys. Res.* A **608** S103
[3] Debus A D *et al* 2010 Electron bunch length measurements from laser-accelerated electrons using single-shot THz time-domain interferometry *Phys. Rev. Lett.* **104** 084802
[4] Lundh O *et al* 2011 Few femtosecond, few kiloampere electron bunch produced by a laser-plasma accelerator *Nature Phys.* **7** 219
[5] Chen S *et al* 2013 MeV-energy x rays from inverse Compton scattering with laser-wakefield accelerated electrons *Phys. Rev. Lett.* **110** 155003
[6] Stupakov G V and Zolotorev M S 2001 Ponderomotive laser acceleration and focusing in vacuum for generation of attosecond electron bunches *Phys. Rev. Lett.* **86** 5274
[7] Kong Q, Miyazaki S, Kawata S, Miyauchi K, Sakai K, Ho Y K, Nakajima K, Miyanaga N, Limpouch J and Andreev A A 2004 Electron bunch trapping and compression by an intense focused pulse laser *Phys. Rev.* E **69** 056502
[8] Karmakar A and Pukhov A 2007 Collimated attosecond GeV electron bunches from ionization of high-z material by radially polarized ultra-relativistic laser pulses *Laser Part. Beams* **25** 371
[9] Bialynicki-Birula I 2004 Particle beams guided by electromagnetic vortices: new solutions of the Lorentz, Schrödinger, Klein–Gordon, and Dirac equations *Phys. Rev. Lett.* **93** 020402
[10] Salamin Y I 2006 Electron acceleration from rest in vacuum by an axicon Gaussian laser beam *Phys. Rev.* A **73** 043402
[11] Fortin P-L, Piche M and Varin C 2010 Direct-field electron acceleration with ultrafast radially polarized laser beams: scaling laws and optimization *J. Phys. B: At. Mol. Opt. Phys.* **43** 025401
[12] Wong L J and Kärtner F X 2010 Direct acceleration of an electron in infinite vacuum by a pulsed radially-polarized laser beam *Opt. Express* **18** 25035
[13] an der Brügge D and Pukhov A 2009 Coherent Thomson scattering at laser compressed and accelerated electron bunches *Proc. SPIE* **7359** 735905
[14] Varin C and Piche M 2006 Relativistic attosecond electron pulses from a free-space laser-acceleration scheme *Phys. Rev.* E **74** 045602
[15] Salamin Y I 2007 Mono-energetic GeV electrons from ionization in a radially polarized laser beam *Opt. Lett.* **32** 90
[16] Marceau V, April A and Piche M 2012 Electron acceleration driven by ultrashort and nonparaxial radially polarized laser pulses *Opt. Lett.* **37** 2442
[17] Marceau V, Varin C and Piche M 2013 Validity of the paraxial approximation for electron acceleration with radially polarized laser beams *Opt. Lett.* **38** 821
[18] Takahashi E J, Kanai T, Ishikawa K L, Nabekawa Y and Midorikawa K 2008 Coherent water window x ray by

phase-matched high-order harmonic generation in neutral media *Phys. Rev. Lett.* **101** 253901

[19] Chen M-C, Arpin P, Popmintchev T, Gerrity M, Zhang B, Seaberg M, Popmintchev D, Murnane M M and Kapteyn H C 2010 Bright, coherent, ultrafast soft x-ray harmonics spanning the water window from a tabletop light source *Phys. Rev. Lett.* **105** 173901

[20] Wang W, Wang P X, Ho Y K, Kong Q, Gu Y and Wang S J 2007 Vacuum electron acceleration and bunch compression by a flat-top laser beam *Rev. Sci. Instrum.* **78** 093103

[21] Sell A and Kärtner F X 2012 Coherent inverse compton scattering with attosecond electron bunches accelerated and compressed by radially polarized laser pulses arXiv:1203.5085[physics.acc-ph]

[22] Cash J R and Karp A H 1990 A variable order Runge–Kutta method for initial value problems with rapidly varying right-hand sides *ACM Trans. Math. Softw.* **16** 201

[23] Barnes J and Hut P 1986 A hierarchical $\mathcal{O}(n \log n)$force calculation algorithm *Nature* **324** 446

[24] Hommelhoff P, Kaelhofer C and Kasevich M A 2006 Ultrafast electron pulses from a tungsten tip triggered by low-power femtosecond laser pulses *Phys. Rev. Lett.* **97** 247402